Journal of Current Science and Technology, April-June 2026 Vol. 16 No. 2, Article 174

ISSN 2630-0656 (Online)

Cite this article: Badr, S. M., Al-Lami, R. A. H., & Al-Shmgani, H. S. (2026). AVCSNPs, a novel alternative antibiotic derived from chitosan nanoparticles loaded with *Aloe vera* flavonoids. *Journal of Current Science and Technology*, *16*(2), Article 174. https://doi.org/10.59796/jcst.V16N2.2026.174

Journal of Current Science and Technology

Journal homepage: https://jcst.rsu.ac.th

AVCSNPs, a novel alternative antibiotic derived from chitosan nanoparticles loaded with *Aloe Vera* flavonoids

Saba Mejdhab Badr[1,*], Rana A.H. Al-Lami[1], and Hanady S. Al-Shmgani[2]

[1]Department of Biology, College of Science for Women/University of Baghdad, Baghdad, Iraq
[2]Biology Department, College of Education for Pure Sciences/Ibn al-Haitham, University of Baghdad, Baghdad, Iraq

Corresponding author; E-mail: Saba.badr2302m@csw.uobaghdad.edu.iq

Received 16 September 2025; Revised 28 October 2025; Accepted 9 November 2025; Published online 30 March 2026

Abstract

The treatment of burn and wound infections is becoming more challenging due to the emergence of antibiotic-resistant bacteria. This study investigated the synergistic antibacterial efficacy of green-synthesized chitosan nanoparticles (CSNPs) loaded with *Aloe vera* gel flavonoid extract (designated AVCSNPs), which were effective against MDR and XDR *Staphylococcus aureus* isolates. The primary goal was to evaluate the antibacterial efficacy of AVCSNPs compared with flavonoid extract alone. Using AVCSNPs as an alternative to antibiotics for Staphylococcus aureus is a low-toxicity and cost-effective approach. The study also examined how AVCSNPs affected the expression of genes associated with antibiotic resistance, such as *mecA* and *aac(6')-Ie-aph(2")-Ia*. Clinical samples were obtained from Ghazi Al-Hariri Hospital and Burns Hospital in Baghdad. The MIC of the flavonoid extract was determined. AVCSNPs were characterized by UV-Vis spectroscopy and particle size analysis after biosynthesis. Using log2-fold change analysis, the effects of treatment on gene expression were investigated. AVCSNPs exhibited greater antibacterial activity than the flavonoid extract, with a MIC of 18.75 µg/mL compared with 50 µg/mL. Studying genes affected by AVCSNPs was essential for understanding antibiotic resistance. Treatment with AVCSNPs significantly reduced the expression of the *mecA* gene, with a mean log2-fold decrease of −14.64. This notable decline indicates that nanoparticles may circumvent the primary resistance mechanism in MRSA bacteria. However, although the decline was less pronounced (−3.37), the expression of the *aac(6')-Ie-aph(2")-Ia* gene also declined. Due to their potent and targeted action on the *mecA* gene, AVCSNPs may be a viable and biocompatible alternative to conventional antibiotics for the treatment of MRSA infections.

Keywords: *chitosan nanoparticles; Aloe vera flavonoids; aac(6')-Ie-aph(2")-Ia; mecA gene; green synthesis; AVCSNPs*

1. Introduction

Antimicrobial resistance (AMR) has become a worldwide health concern, with multidrug-resistant (MDR) infections expected to cause 10 million fatalities per year by 2050 (World Health Organization, 2022). *Staphylococcus aureus* is one of the most virulent bacteria because it thrives in chronic wounds and burns, posing a significant concern for healthcare professionals. Genes such as *mecA*, which encodes the PBP2a protein and confers methicillin resistance (Fishovitz et al., 2014), and *aac(6')-Ie-aph(2")-Ia*, which produces modifying enzymes and confers gentamicin resistance (Hauschild et al., 2008), significantly affect bacterial resistance to antibiotics. Flavonoids derived from *Aloe vera*, such as luteolin, quercetin, and kaempferol, have been identified as promising candidates due to their antibacterial activity and synergistic anti-inflammatory properties (Al-Kubaisi et al., 2020; Kadium et al., 2023). Flavonoids are a wide range of phenolic compounds produced as secondary metabolites in plants, bacteria, and fungi (Gidamo, 2024). However, pharmacokinetic obstacles, including poor water solubility, metabolic instability, and restricted absorption, constrain their practical use

(Jafar et al., 2024). A nanotechnology-based solution using green-synthesized chitosan nanoparticles (CSNPs) presents an effective strategy to address these constraints by enhancing stability, bioavailability, and targeted delivery of these phytochemicals (Ausaj et al., 2024; Al-Musawi et al., 2022). Even with these improvements, the combined antibacterial effect of *Aloe vera* flavonoid-loaded chitosan nanoparticles (AVCSNPs) against MDR/XDR wound infections remains unclear. This work aims to bridge this gap by isolating and characterizing flavonoids from *Aloe vera*, synthesizing AVCSNPs, and subsequently evaluating their synergistic antibacterial activity against clinically significant *S. aureus* to clarify the underlying mechanisms of action. This study aims to provide a biocompatible, scalable, and effective alternative to traditional antibiotics, addressing a significant unmet need in managing infections that are resistant to treatment.

2. Objectives

In this study, we aim to evaluate:

1. Using UV-Vis spectroscopy and particle size analysis, chitosan nanoparticles (CSNPs) are synthesized and characterized, and their physicochemical properties are examined after loading with Aloe vera gel flavonoid extract to produce AVCSNPs.

2. Determine the minimum inhibitory concentration (MIC) of AVCSNPs and Aloe vera gel flavonoid extract alone to compare their antibacterial activity against MDR and XDR *Staphylococcus aureus* isolates.

3. Investigate the effects of AVCSNPs on the expression of genes linked to antibiotic resistance in resistant *Staphylococcus aureus* isolates, including *mecA* and *aac(6')-Ie-aph(2")-Ia.*

4. Evaluate the biocompatibility, low-toxicity profile, and antibacterial effectiveness of AVCSNPs as a cost-effective alternative to conventional antibiotics for treating MRSA and MDR/XDR infections.

3. Materials and Method

3.1 Collection and Identification of Bacterial Isolates

A total of 150 clinical samples were collected in Iraq. The isolates included MDR and XDR strains of *S. aureus*. Bacterial identification was performed using Gram staining and biochemical tests (e.g., catalase, oxidase, and coagulase). Molecular confirmation was performed using 16S ribosomal RNA (rRNA) gene sequencing for isolates with ambiguous identification (Urtgam et al., 2024). Antibiotic susceptibility testing using the Kirby-Bauer disk diffusion method (CLSI guidelines) was performed to classify MDR/XDR strains. The antibiotic susceptibility of *Staphylococcus aureus* was assessed (El-Naggar et al., 2022). The study involved 28 isolates of *S. aureus* tested against 14 antibiotics by measuring the diameter of the inhibition zone in millimeters, following CLSI 2024 criteria and referencing the primary source (Humphries et al., 2021). The isolates showed resistance to the following antibiotic classes: Macrolides (Erythromycin 15 mg), Penicillin (Penicillin 10 mg, Cefoxitin 30 mg, Oxacillin 1 mg), Aminoglycosides (Gentamicin 10 mg), and Fluoroquinolones (Ciprofloxacin 5 mg, Levofloxacin 5 mg). Conversely, they exhibited intermediate resistance to Tetracycline (Tetracycline 30 mg), Folate pathway antagonists (Trimethoprim 5 mg), the Oxazolidines class (Linezolid 30 mg), the Phenicols class (Chloramphenicol 30 mg), the Nitrofurantoin class (Chloramphenicol 30 mg, Penicillin 10 mg), the Ansamycins class (Rifampin 5 mg), and the Lincosamides class (Clindamycin 23 mg).

This study was conducted in accordance with ethical guidelines and approved by the Sciences College for Women, University of Baghdad, Baghdad, Iraq (document number 22/7269, dated November 5, 2024). All clinical samples were collected with appropriate permissions from Ghazi Al-Hariri Hospital and Burns Hospital in Baghdad, Iraq. Patient confidentiality and data privacy were strictly maintained, and no personal identifiers were linked to the samples.

3.2 Extraction of *Aloe vera* Flavonoids

Plant material: Fresh aloe leaves were used. The leaves were cut and washed, and the gel was removed from the epidermis using a spoon. The gel was then placed in containers and dried in an oven at 45°C ± 5°C for 24 hours. The dried samples were then ground into powder and stored in clean, dried, sealed containers at room temperature for further analysis (Prisa, 2022).

3.3 Green Synthesis of Chitosan Nanoparticles (AVCSNPs)

The green synthesis of chitosan nanoparticles employed the ionic gelation method with TPP, as described by Villarta et al. (2025). First, a 0.2% chitosan solution was prepared in 1% acetic acid, with a pH of ~3.5. The solution was then evaporated and condensed for one hour using a Dean-Stark apparatus. Chitosan powder (200 mg) was then dissolved in 100 mL of acetic acid. The *Aloe vera* flavonoid extract was prepared by mixing 7.5 mL of *Aloe vera* extract with 10 mL of dimethyl sulfoxide (DMSO). Moreover,

xylene (50 mL) was added to the chitosan solution. Using a Dean-Stark apparatus, xylene and the flavonoid extract were added dropwise to chitosan dissolved in acetic acid. The mixture was centrifuged at 6,000 rpm for 20 min. The precipitated product was dissolved in a 1% acetic acid solution under stirring and heating, serving as a reducing and stabilizing agent. The precipitate was then resuspended in water, dried at 50 °C in an oven, and stored at 4 °C for further use.

3.4 Characterization of AVCSNPs

To confirm the formation of nanoparticles (NPs), UV-Vis spectrophotometry, with a wavelength range of 200–800 nm, was used to determine their absorption. Fourier Transform Infrared Spectroscopy (FTIR) (4000–400 cm^{-1}, 4 cm^{-1}) was employed using a SHIMADZU spectrometer (Japan) to characterize the functional groups of chitosan and AVCSNPs. Samples were prepared as KBr pellets (1:99 sample-to-KBr ratio) for analysis, and characteristic X-rays were emitted by the sample under electron beam irradiation. Moreover, crystallinity and phase structure were examined via X-ray diffraction (XRD) (Cu-Kα radiation, λ = 0.15406 nm, 40 kV, 30 mA); samples were dried, mounted on a silicon substrate, and scanned over a 2θ range of 10°–80° at room temperature (SHIMADZU-XRD-6000/ Japan), and particle size was determined by DLS (Dynamic Light Scattering) (Brookhaven Instruments Corp., USA).

3.5 Determination of Flavonoid Compounds in the Extract and AVCSNPs using the HPLC Technique

High-Performance Liquid Chromatography (HPLC) was used to identify and quantify the principal flavonoids in both the aloe gel extract and the synthesized AVCSNPs. Following methodologies derived from Ali (2022), analysis was performed using a SYKAMN HPLC system (Germany). The mobile phase consisted of two solvents: Solvent (A), 0.05% trifluoroacetic acid in deionized water, and Solvent (B), 0.05% trifluoroacetic acid in methanol. Separation was achieved using gradient elution. Detection was carried out at a wavelength of 280 nm with a constant flow rate of 1.1 mL/min. A standard calibration curve was constructed using six flavonoid standards (quercetin, kaempferol, apigenin, catechin, coumarin, and rutin), each at a concentration of 25 µg/mL. The concentration of each flavonoid in the samples was calculated using the following equation:

$$\text{Concentration (mg/mL)} = (AC / AS) \times C \times D$$

where AC = peak area of the samples, AS = peak area of the standard, C = concentration of the standard solution (mg/mL), and D = dilution factor of the samples

3.6 Antibacterial Susceptibility Testing

Following CLSI 2024 guidelines for Kirby-Bauer disk diffusion antimicrobial susceptibility testing and antibacterial activity assays, the antibacterial efficacy of AVCSNPs was evaluated against antibiotic-resistant bacteria using the minimum inhibitory concentration (MIC) assay. The MIC was determined via a resazurin-assisted microdilution method in 96-well plates containing Mueller-Hinton broth (MHB) (Jirakitticharoen et al., 2022). Positive control (bacterial suspension alone) and negative control (MHB alone) were included. Each well was filled with 180 µL of broth medium, and serial dilutions of the bacterial inoculum (10 µL) and experimental material (10 µL) (one plate for flavonoids and another for AVCSNPs) were added to each well. The plates were then incubated at 37°C for 24 h. Wells with a blue resazurin color indicated bacterial growth inhibition above the MIC and minimum bactericidal concentration (MBC).

3.7 Genotyping Detection

3.7.1 DNA Template Preparation by the Boiling Method:

The DNA template was prepared using a boiling method adapted from Ali et al. (2018). Briefly, five isolated colonies from overnight bacterial growth were thoroughly suspended in 2 mL of distilled water and boiled in a water bath for 10 minutes. After centrifugation, the supernatant was collected and used as template DNA for subsequent PCR amplification.

3.7.2 PCR Amplification

PCR amplification was performed for the genetic detection of local *Staphylococcus aureus* isolates (Choi et al., 2003; Mehrotra et al., 2000). The final volume for each uniplex PCR mixture was 25 µL, consisting of 12.5 µL of 2× Master Mix, 5 µL of template DNA, 1 µL each of forward and reverse primers, and 5.5 µL of nuclease-free water. Volumes were adjusted for multiplex PCR. Reaction mixtures were briefly mixed using a vortex and then placed in a thermal cycler. Annealing temperatures and cycling conditions for each PCR mixture are detailed in Table 2. Primer oligonucleotide sequences used in this study are listed in Table 1.

Table 1 Primer Oligonucleotide Sequences Used in This Study

Primer	Direction	5 → 3	Size bp
16s	F	GTGGGGAGCAAACAGGATTA	213
	R	TAAGGTTCTTCGCGTTGCTT	
aac(6')-Ie-aph(2")-Ia	F	CAGAGCCTTGGGAAGATGAAG	348
	R	CCTCGTGTAATTCATGTTCTGGC	
mecA	F	ACTGCTATCCACCCTCAAAC	163
	R	CTGGTGAAGTTGTAATCTGG	

Note. F = forward primer; R = reverse primer. Size (bp) refers to the expected PCR amplicon size, not the primer length.

Table 2 Amplification Program of Primers

Amplified gene	Initial denaturation	No. of cycle	Denaturation	Annealing	Elongation	Final extension
aac(6')-Ie-aph(2")-Ia	95°C/ 7min	35	94°C/ 40 sec	53°C/40 sec	72°C/60 sec	72°C/2min
mecA	95°C/ 4min	40	94°C/ 40 sec	63°C/40 sec	72°C/60 sec	72°C/5min

3.7.3 Primer Dilution

Lyophilized oligonucleotide primers were initially dissolved and diluted in nuclease-free, distilled, sterile deionized water (D.S.D.W.) according to the manufacturer's recommendations to achieve a 100 pmol/µL stock solution. This stock was then further diluted in nuclease-free D.D.W to a working concentration of approximately 10 pmol/µL. This dilution technique was consistently applied to all primers used in this study. Primer specifications for all genes were obtained from Alpha DNA Company, USA.

3.7.4 Agarose Gel Electrophoresis

Amplified PCR products were detected by agarose gel electrophoresis and visualized using ethidium bromide dye and a UV transilluminator documentation system. Briefly, 1 g of agarose was added to 100 mL of 1× TBE buffer. TBE buffer was added to cover the gel, and electrophoresis was performed for 1 hour at 5 V/cm² for both the DNA extract and PCR products (Huanbutta et al., 2023). After electrophoresis, the agarose gel was removed from the tank, visualized using a UV transilluminator documentation system, and photographed with a digital camera (Mishra et al., 2010). Each well was loaded with 5 µL of the monoplex PCR products (Morovat et al., 2009). DNA ladders were consistently run concurrently with each electrophoretic run to determine the size of the PCR products.

3.8 cDNA Synthesis and RT-qPCR Protocol

3.8.1 RT-qPCR Protocol

Total RNA samples were thawed, and 10 µL from each extracted sample was added to a new PCR tube. Four microliters of cDNA Master mix (containing dNTPs, buffer, and essential components) were added per sample. The final volume was adjusted to 20 µL by adding 6 µL of ddH_2O. The mixture was briefly centrifuged. The reaction was then amplified and annealed at 25°C for 10 minutes, followed by an extension at 42°C for 15 minutes, and finally, reverse transcriptase was heat-inactivated at 85°C for 5 seconds.

3.8.2 Quantitative PCR

cDNA samples from bacteria and the control were subjected to quantitative PCR in the same run. Each sample was prepared in triplicate, with separate PCR tubes designated for *mecA*, *aac(6')-Ie-aph(2")-Ia*, and 16S rRNA (used as a housekeeping gene). Quantitative detection was based on the fluorescent intensity of SYBR Green dye, which binds double-stranded DNA and emits fluorescence proportional to the amount of PCR product generated. The 20 µL reaction mixture components and their quantities are detailed in Table 3.

Table 3 Components of RT-PCR Reaction (20 µL Total Volume)

Component	Quantity (µL)
2× Universal Super SYBR Master Mix	10
Forward primer (10 µM)	0.5
Reverse primer (10 µM)	0.5
Template DNA	2
Nuclease-free Water	7

PCR tubes were rapidly centrifuged (1 minute at 2000 × g) to remove bubbles and collect the liquid (Aldhahir et al., 2025). The real-time PCR program was set up using the thermocycling protocol outlined in Table 4.

Table 4 RT-PCR Conditions

Cycle Step	Temperature (°C)	Time	Cycles
Initial denaturation	95	30 seconds	1
Denaturation	95	15 seconds	45
Annealing	55	30 seconds	
Extension	72	30 seconds	
Melting curve	95	1 minute	1
	60	30 seconds	
	95	30 seconds	

3.8.3 Gene Expression Analysis

Quantitative real-time PCR (qRT-PCR) data were analyzed by directly comparing the cycle threshold (Ct) values of the target genes (*mecA* and *aac[6']-Ie-aph[2"]-Ia)* with those of the reference gene (16S rRNA). Gene expression levels were assessed using the relative quantification method, specifically the Livak formula (Al-Khafaji & Al-Hayawi, 2024), as described below:

The ΔCt of the target gene relative to the reference gene was calculated for each sample (unknown and calibrator) as follows:

$$\Delta Ct = CT \text{ target gene} - Ct \text{ reference gene}$$

the difference in ΔCt values between the unknown samples and the calibrator (control) was determined using the following equation:

$$\Delta\Delta Ct = (Ct \text{ target gene} - Ct \text{ reference gene}) \text{ sample} - (Ct \text{ target gene} - Ct \text{ reference gene}) \text{ control}$$

the normalized target quantity for each sample was calculated as $2^{(-\Delta\Delta Ct)}$. This value represents the fold change in gene expression levels and was used for comparative analysis:

$$\text{Fold change} = 2^{(-\Delta\Delta Ct)}$$

relative changes in mRNA expression levels between antibiotic-treated and untreated bacterial isolates were measured using the comparative threshold cycle (Ct) value method.

3.9 Statistical Analysis

Data were analyzed using SPSS and R software. Statistical analysis included descriptive statistics, one-way ANOVA, and post-hoc comparisons with the least significant difference (LSD) test. Data preprocessing and visualization, including the creation of bar and violin plots, were conducted in R using the `dplyr`, `ggplot2`, and `ggpubr` packages.

4. Results and Discussion

4.1 Identification of Bacterial Isolates

A total of 150 clinical samples were collected from Iraqi hospitals in Baghdad. Extensively drug-resistant (XDR) and multidrug-resistant (MDR) *Staphylococcus aureus* strains were among the isolates. Gram stain analysis and biochemical tests, as detailed in Table 5, including catalase, oxidase, and coagulase, identified the isolates and confirmed bacterial identity through a battery of standard tests.

Table 5 Biochemical tests

Characteristics	*S. Aureus*
Coagulase	Positive
Oxidase	Negative
Catalase	Positive

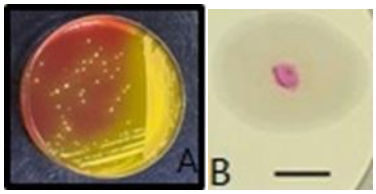

Figure 1 (A) S. aureus on mannitol agar producing golden-yellow colonies; (B) Oxidase-negative result.

By targeting specific genes, polymerase chain reaction (PCR) is a crucial diagnostic tool that enables accurate identification of bacteria. In this study, the highly conserved 16S rRNA gene was amplified using PCR to confirm the presence of *Staphylococcus aureus*. Clear and distinct bands, matching the expected size of 565 base pairs, were visible in the sample lanes, indicating successful amplification. The clear separation of these bands indicates the absence of significant contamination or degradation, confirming the effectiveness of the PCR method.

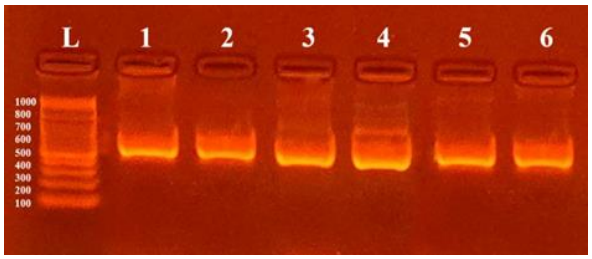

Figure 2 Gel electrophoresis of the amplified PCR product of 16S rRNA (565 bp) from *S. aureus*. Lane L: 1000 bp DNA ladder; lanes 1–4: 16S bands

Significant differences ($P < 0.001$) in antibiotic susceptibility to 14 antibiotics were found among the 28 *S. aureus* isolates subjected to Kirby-Bauer disk diffusion analysis. In Figure 3, Inhibition zones around the disks were measured to determine whether the isolates were resistant or sensitive to the antibiotics.

All isolates were resistant to both oxacillin and penicillin. According to the World Health Organization (WHO, 2022) and Al-Lami et al. (2022), resistance to cefoxitin and oxacillin is a global indicator of MRSA. In Table 6 and Figure 4, cefoxitin had a 75% resistance rate, which was significantly higher than that of other antibiotics. Between 68% and 96% of isolates were resistant to gentamicin, erythromycin, ciprofloxacin, and levofloxacin. Zhang (2018) reported that clinical isolates were becoming increasingly resistant to fluoroquinolones and macrolides. With sensitivity rates of 100% and 96.43%, respectively, nitrofurantoin and chloramphenicol demonstrated superior efficacy. The sensitivity of rifampin, clindamycin, and linezolid ranged from 92.86% to 89.29%. Vercelli (2023) and Eckmann & Dryden (2010) reported comparable MRSA and *S. aureus* susceptibility patterns. Contrary to our findings, Mendem et al. (2016) found significant resistance to gentamicin, tetracycline, clindamycin, chloramphenicol, and rifampin in some locations. Continuous antibiotic susceptibility testing is crucial due to rising resistance rates, which make treating *S. aureus* infections more challenging (WHO, 2022).

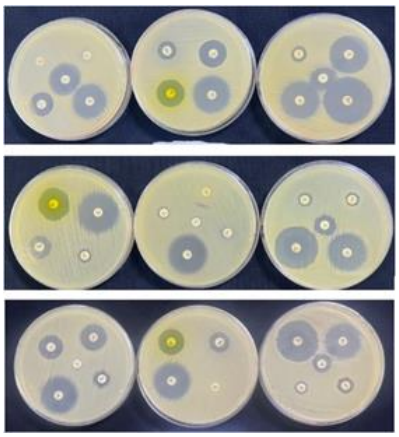

Figure 3 Antibiotic susceptibility test for *S. aureus* and the antibiotic resistance range according to CLSI (2024) parameters

Table 6 Antibiotic susceptibility test for 28 *Staphylococcus aureus* isolates

Antibiotic	Total No. of isolates	Resistant		Intermediate		Sensitive		Chi (χ^2)	P value
		No.	%	No.	%	No.	%		
Tetracycline (30) mg	28	15	53.57%	0	0%	13	46.43%	0.14	0.7 NS
Ciprofloxacin (5 mg)	28	20	71.43%	1	3.57%	7	25%	20.21	<0.001**
Gentamicin (10 mg)	28	22	78.57%	3	10.71%	3	10.71%	25.78	<0.001**
Erythromycin (15 mg)	28	27	96.43%	1	3.57%	0	0%	24.14	<0.001**
Linezolid (30 mg)	28	0	0%	3	10.71%	25	89.29%	17.29	<0.001**
Chloramphenicol (30 mg)	28	1	3.57%	0	0%	27	96.43%	24.14	<0.001**
Nitrofurantoin (300 mg)	28	0	0%	0	0%	28	100%	-	-
Cefoxitin (30 mg)	28	21	75%	1	3.57%	6	21.43%	23.21	<0.001**
Oxacillin (1 mg)	28	28	100%	0	0%	0	0%	-	-
Levofloxacin (5 mg)	28	19	67.86%	1	3.57%	8	28.57%	17.64	<0.001**
Rifampin (5 mg)	28	2	7.14%	0	0%	26	92.86%	20.57	<0.001**
Clindamycin (23 mg)	28	1	3.57%	1	3.57%	26	92.86%	44.64	<0.001**
Penicillin (10) mg	28	28	100%	0	0%	0	0%	-	-
Trimethoprim (5 mg)	28	10	35.71%	0	0%	18	64.29%	2.28	0.13 NS
Chi (χ^2)	-	72.84		3.63		56.58		-	
P value		<0.001**		0.7 NS		<0.001**			

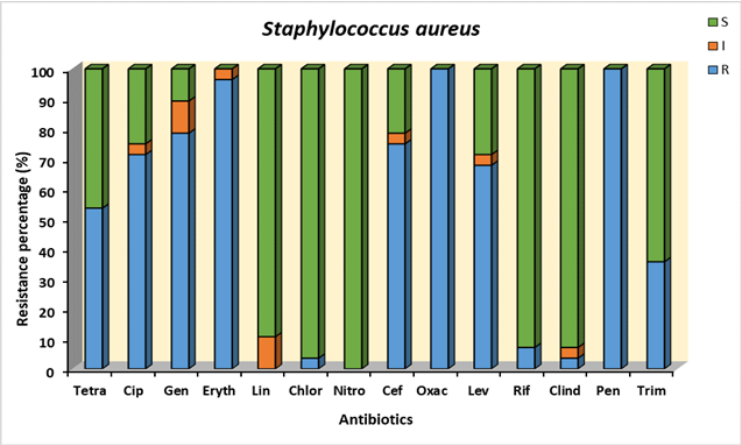

Figure 4 Antibiotic sensitivity testing of *S. aureus*

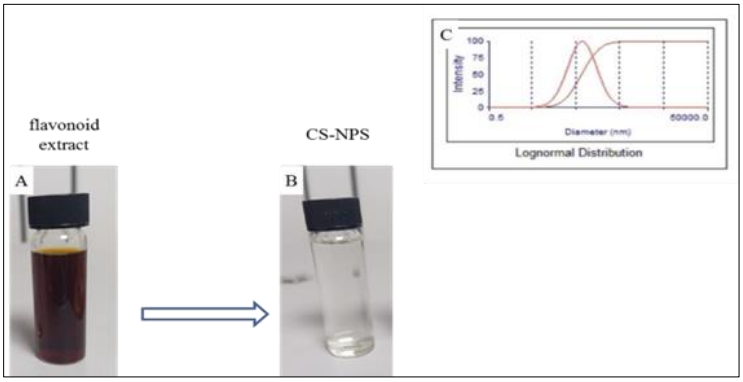

Figure 5 Synthesis of chitosan nanoparticles (AVCSNPs) color change: (A) flavonoid extract, (B) AVCSNPs, and inset (C) particle size distribution by Dynamic Light Scattering (DLS)

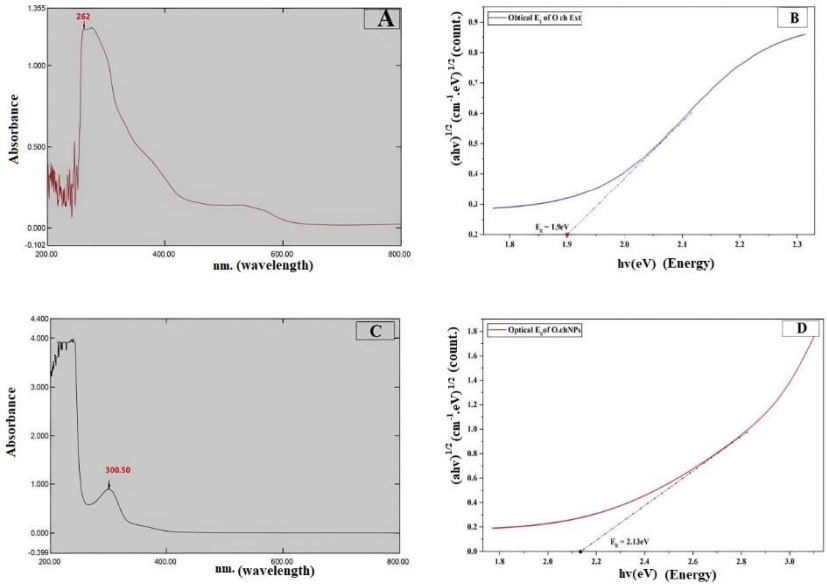

Figure 6 UV-spectrophotometric analysis showed the absorption peaks of (A) flavonoid extract and (C) AVCSNPs. (B) and (D) show the optical band gap of flavonoid extract and AVCSNPs, respectively.

4.2 Preparation and Characterization of AVCSNPs

As shown in Figure 5, the dark reddish-brown coloration of the flavonoid extract indicates that unformulated plant polyphenols exhibit intrinsic chromophoric characteristics. In contrast, the AVCSNPs solution appears clear and transparent. The average effective particle diameter was 68.9 ± 27.9 nm, and the polydispersity index (PDI) was 0.772. The lognormal intensity distribution map indicates that the particles are dispersed across a wide range of values (inset, Figure 5).

UV-Vis results of AVCSNPs revealed a peak at 300 nm (Figure 6C), while the raw flavonoid extract exhibited peaks at 262 nm (Figure 6A). The flavonoid extract B-Tauc plot estimated the optical band gap at 1.9 eV (Figure 6B). The CS-NPs B-Tauc plot estimated the optical band gap at 2.13 eV (Figure 6D).

FTIR results included a broad range of O–H stretching (3200-3600 cm^{-1}), C=O stretching (1650-1750 cm^{-1}), aromatic C=C vibrations (1450-1650 cm^{-1}), and C–O stretching (1000-1200 cm^{-1}), with CS-NPs showing notable changes in the spectral data. Characteristic chitosan peaks, such as the broad O–H/N–H stretch around 3000-3500 cm^{-1}, the amide II band around 1580-1600 cm^{-1}, and the C–O–C polysaccharide stretches around 1000-1150 cm^{-1}, are observed in Figure 7.

XRD results in Figure 8 demonstrate the crystal structure of the synthesized particles, with peaks observed at 2θ values ranging from 20 to 40 degrees, indicating the presence of ordered crystalline domains. The highest peak was at 34.61°, while the other peaks were at 24.52°, 26.63°, 30.22°, 33.37°, and 38.64°.

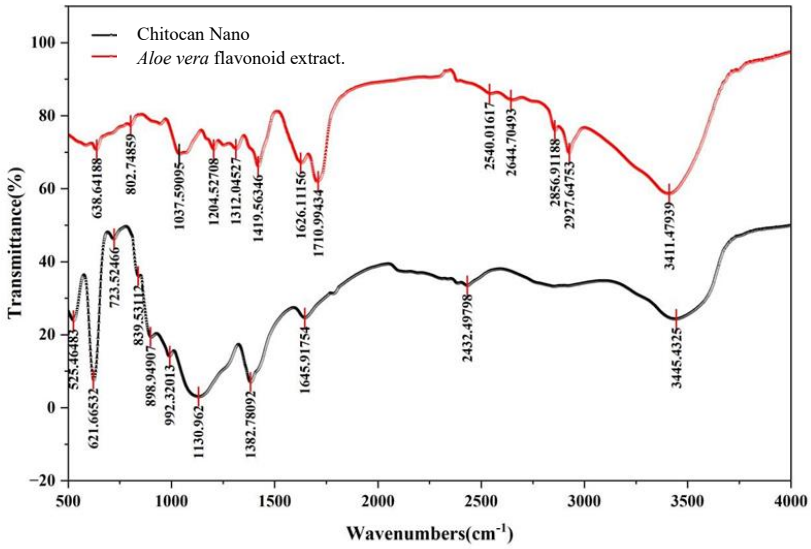

Figure 7 Comparative Fourier-transform infrared (FTIR) analysis of chitosan nanoparticles (black line) and flavonoid extract (red line)

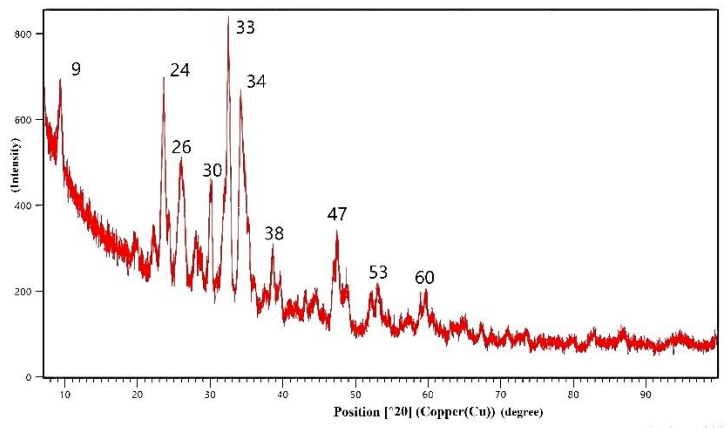

Figure 8 X-ray diffraction of AVCSNPs

This study verified the structural characteristics and successful formation of *Aloe vera* flavonoid-loaded chitosan nanoparticles (AVCSNPs). The flavonoids underwent a chemical change and were successfully entrapped within the chitosan matrix, as demonstrated by UV-Vis spectroscopy. The successful integration of flavonoids into the nanoparticles was confirmed by the appearance of new peaks in the AVCSNPs spectrum and the disappearance of prominent peaks in the raw extract. These results were confirmed by Tauc plot analysis, which revealed a shift in the optical band gap from 1.9 eV for the raw extract to 2.13 eV for the AVCSNPs. This suggests that the interaction between the flavonoids and chitosan at the nanoscale level changed the electronic structure. Furthermore, Fourier-transform infrared (FTIR) spectroscopy confirmed that the functional groups of the flavonoids were integrated into the chitosan framework, as evidenced by the appearance of new peaks and modifications to preexisting ones, providing compelling evidence of chemical interactions between the constituents. Lastly, X-ray diffraction (XRD) analysis confirmed that the AVCSNPs retained a semicrystalline structure. This suggests that the nanofabrication process did not adversely affect the polymer's basic structural characteristics but rather helped preserve both its crystalline and amorphous phases, in line with previous studies in this area (Kiani, 2023). Together, these findings demonstrate that the flavonoids were effectively incorporated into the chitosan nanoparticles, indicating the efficacy of the nanofabrication technique employed in this investigation, which aligns with the study by Akdaşçi et al. (2025).

4.3 Determination of Flavonoid Compounds in the Extract and AVCSNPs using the HPLC Technique

In Table 7, the original extract contained 128.7 mg of flavonoids per 100 g, whereas the synthesized chitosan nanoparticles (AVCSNPs) contained 83.2 mg of flavonoids per 100 g. The original amount of active compounds in the raw extract was 128.7 mg/100 g. The amount retained in the nanoparticles was 83.2 mg/100 g. AVCSNPs often have a lower flavonoid concentration because encapsulation is not always complete, and some material is lost during preparation or partial loading. This result indicates that the encapsulation efficiency is approximately 64.6% ((83.2/128.7) x 100), which is consistent with what is expected for this type of procedure. Chitosan and the flavonoids within the AVCSNPs comprise the total mass of these nanoparticles. This means that there are fewer flavonoids in this than in the pure extract. The primary goal of nanoencapsulation is not to increase concentration but to enhance properties such as solubility, stability, prolonged release, bioavailability, and targeted delivery. This is why the final product has a lower concentration than the pure extract (Ali, 2022).

4.4 In Vitro Evaluation of the Antibacterial Activity of AVCSNPs

A microtiter plate experiment using resazurin dye was employed to evaluate the antibacterial activity of AVCSNPs and flavonoids against *S. aureus* (Figure 9). The transition of the dye from purple, signifying bacterial growth inhibition, to pink when bacteria were growing was used to ascertain the minimum inhibitory concentration (MIC). The resazurin microplate assay was used in the MIC test because it is a rapid, objective, high-throughput, quantitative, and cost-effective method that is accurate, reliable, sensitive, and user-friendly. The test is quantitative and based on metabolic activity and cellular vitality. The non-fluorescent blue dye (resazurin) is reduced to the fluorescent pink dye (resorufin) by reductases in specific cellular organelles (O'Brien et al., 2000). It allows the detection of microbial growth in small volumes of solutions in microtiter plates without requiring a spectrophotometer (Hussain et al., 2011). The resazurin test uses color change after incubation, compared with a control, to demonstrate an antibacterial effect. It has also been used to evaluate the antibacterial activity of various phenolic and flavonoid compounds (Bouslamti et al., 2022). Several studies have investigated the effects of plant extracts or essential oils on both Gram-negative and Gram-positive bacteria, demonstrating their superiority over the disk diffusion method. AVCSNPs have shown significant efficacy against *S. aureus*, with a minimum inhibitory concentration (MIC) of 18.75 µg/mL, whereas flavonoids showed a MIC of 50 µg/mL (Table 7).

The resazurin test is a dependable and economical technique for evaluating antibacterial characteristics based on bacterial metabolic activity (Karuncharoenpanich et al., 2025), particularly for natural compounds such as flavonoids, which are known for their extensive effects (Cushnie & Lamb, 2011; Faiq & Ahmed, 2024).

Table 7 Comparison between total flavonoid in AVCSNPs and in the extract

Total Flavonoid In AVCSNPs and in the extract	Extract	Chitosan nanoparticles AVCSNPs
	128.7 mg/100 g	83.2 mg/100 g

Table 8 Determination of minimum inhibitory concentration (MIC) using the MTP method (- no growth, + growth)

Concentration Of AVCSNPs µg/mL	*S.aureus*	Concentration of Flavonoids µg/mL	*S.aureus*
Control	-	Control	-
37.500	-	100.000	-
18.750	– (MIC)	50.000	–(MIC)
9.375	+(Sub-MIC)	25.000	+(Sub-MIC)
4.687	+	12.500	+
2.343	+	6.250	+
1.171	+	3.125	+
0.585	+	1.562	+
0.292	+	0.781	+
0.146	+	0.390	+
0.073	+	0.195	+

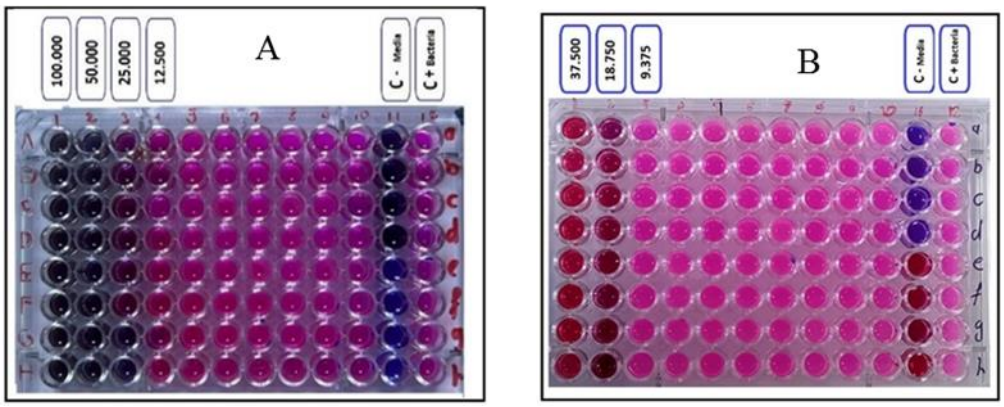

Figure 9 Microtiter plate assay demonstrates the antibacterial activity of (A) flavonoid extract and (B) AVCSNPs against *S. aureus*

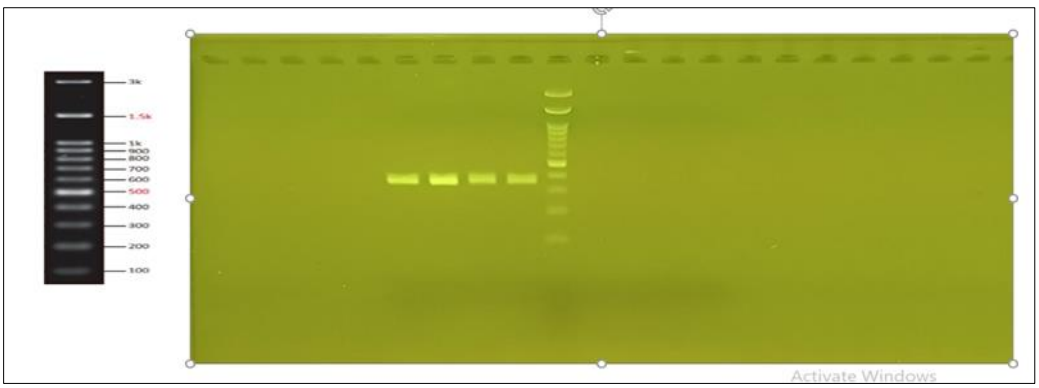

Figure 10 Agarose gel electrophoresis (1.5% agarose, 7V/cm² for 60 min) for *aac(6')-Ie-aph(2")-Ia* gene (348 bp amplicon), lane 100 bp DNA Ladder

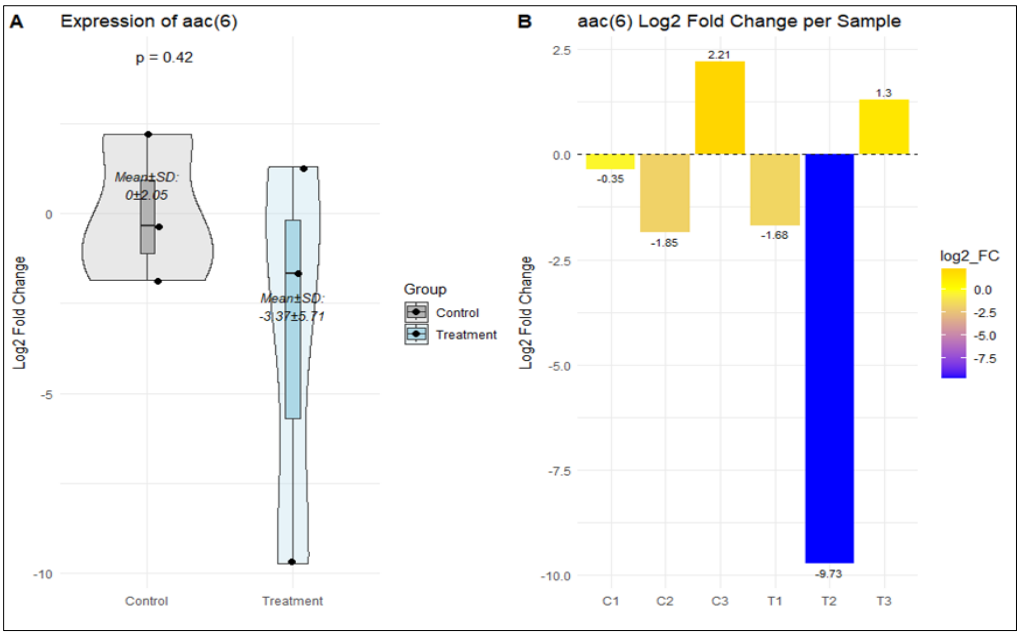

Figure 11 Gene expression of *aac(6')-Ie-aph(2'')-Ia* Gene

4.5 PCR Amplification

4.5.1 Gene: aac(6')-Ie-aph(2")-Ia

PCR amplification confirmed the presence of the *aac*(6′)-*Ie-aph*(2″)-*Ia* gene in the resistant isolates. Agarose gel electrophoresis (1.5% agarose, 7 V/cm² for 60 min) revealed clear and distinct bands at the expected amplicon size of 348 bp, with no non-specific bands observed, indicating successful and specific amplification (Figure 10). The presence of this gene confirms that the isolates carry the bifunctional enzyme responsible for aminoglycoside modification, which confers gentamicin resistance.

4.5.2 Gene: mecA

PCR amplification confirmed the presence of the *mecA* gene in the resistant isolates. Agarose gel electrophoresis revealed a distinct band at the expected amplicon size of 163 bp (Figure 11). The detection of *mecA*, which encodes the penicillin-binding protein PBP2a, confirms the methicillin-resistant phenotype of the *S. aureus* isolates and classifies them as MRSA. These genotyping results are consistent with the phenotypic resistance patterns observed in the Kirby-Bauer disk diffusion results in Section 4.1, where 100% of isolates were resistant to oxacillin and penicillin.

4.6 Quantitative PCR

4.6.1 Gene: aac(6')-Ie-aph(2")-Ia

The *aac(6')-Ie-aph(2")-Ia* gene expression was generally downregulated following treatment with *Aloe vera* flavonoid-loaded chitosan nanoparticles (AVCSNPs) (Figure 12). The high standard deviation (± 5.11) indicates substantial variability across isolates. The overall mean log2-fold change of –3.37 ± 5.11 indicates that AVCSNPs reduced expression of the *aac(6')-Ie-aph(2")-Ia* resistance gene. The control group's mean was 0 ± 2.05. The nanoform can nearly stop production of the bifunctional enzyme encoded by *aac(6')-Ie-aph(2")-Ia* in some isolates, as shown by sample T3 (–9.73 log2-fold change). This might restore aminoglycoside efficacy. Sample T1 (–1.68 log2-fold change) showed a marked decrease in expression, whereas sample T2 (+1.30 log2-fold change) showed an increase. This variability makes it difficult to interpret the treatment response across isolates. The *aac(6')-Ie-aph(2")-Ia* gene is likely located on different mobile genetic elements (MGEs), such as plasmids or the transposon Tn4001, which may alter its genomic position (chromosomal or plasmid) or gene copy number.

A sub-inhibitory dose of AVCSNPs may act as an inducer rather than an inhibitor. This may be because isolate T2 has compensatory mechanisms that flavonoids do not affect, such as changes in outer membrane permeability or increased efflux pump activity that prevent nanoparticles from reaching intracellular targets. According to Amini et al. (2024), this discrepancy, along with the absence of statistical significance ($p = 0.42$) indicates that the observed variation in gene expression is not attributable to treatment alone and likely reflects distinct regulatory mechanisms.

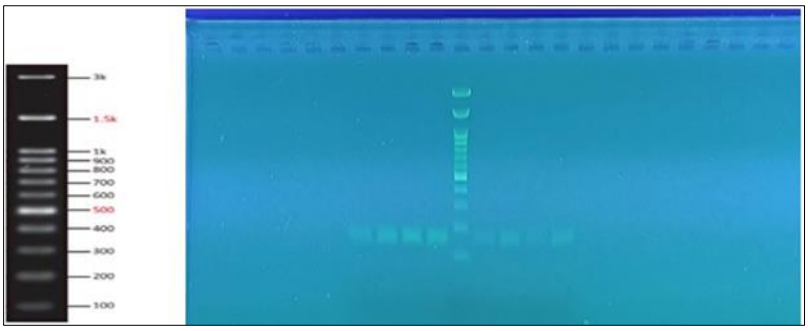

Figure 12 Agarose gel electrophoresis (1.5% agarose, 7 V/cm² for 60 min) for the *mecA* gene (163 bp amplicon), lane: 100 bp DNA ladder

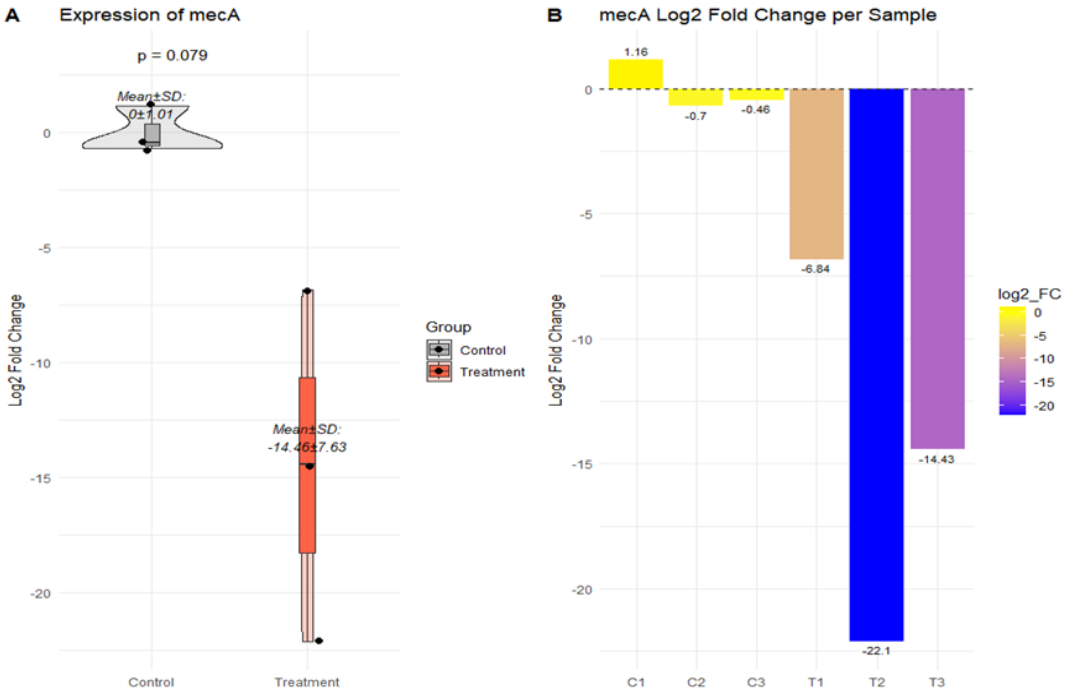

Figure 13 Gene expression of the *mecA* Gene

4.6.2 Gene: mecA

The decrease in *mecA*, as observed in Figure 13, which was evident shortly after AVCSNP therapy, although not statistically significant, suggests that the treatment could be a novel approach to combating resistance. The treatment group exhibited a crucial biological effect, as evidenced by a substantial decrease in expression, with an average log2-fold change of –14.64 ± 7.63. The control group, in contrast, did not vary substantially from its initial value (0.41 ± 1.07). This –14.64 log2-fold change means that the *mecA* gene transcript decreased by approximately 25,850-fold. This suggests that the genetic mechanism underlying methicillin resistance is almost completely disrupted. A key goal of anti-resistance treatment strategies is to achieve *mecA* repression at this level. This could render Methicillin-Resistant *Staphylococcus aureus* (MRSA) strains susceptible to beta-lactam antibiotics, thereby shifting them toward a Methicillin-Sensitive *Staphylococcus aureus* (MSSA)-like phenotype. This discovery supports earlier studies showing that phytochemicals

can disrupt *mecA* regulation and MRSA pathogenesis (Ender et al., 2008; Rahman et al., 2024). The *p*-value of 0.079 is higher than the usual threshold for statistical significance ($p < 0.05$); therefore, the results should be interpreted cautiously, and further research is needed. The standard deviation is high (± 7.63), indicating substantial variability across isolates. The reductions ranged from –6.84 to –22.1 log2-fold change. The variations were likely due to differences in the staphylococcal cassette. The release of the flavonoid payload to the *mecA* promoter may be contingent upon regulatory elements present in clinical isolates, including SCCmec types that influence *mecA* transcription. The variations in transcriptional response may be attributed to distinct mechanisms by which different bacterial strains internalize nanoparticles and subsequently release flavonoids. The lack of statistical significance regarding the therapeutic potential of AVCSNPs is primarily due to the small sample size and the inherent variability of clinical isolates. To address this statistical concern and confirm the observed biological effect, further studies of larger sample sizes are needed.

5. Conclusion

The rise of MDR and XDR bacteria, such as *Staphylococcus aureus*, necessitates the development of new treatments for burn and wound infections. This study evaluated the synergistic antibacterial efficacy of green-synthesized chitosan nanoparticles (CSNPs) loaded with Aloe vera gel flavonoid extract (AVCSNPs) using clinical isolates. The study's objectives were to assess the impact of AVCSNPs on antibiotic resistance genes, such as *mecA* and *aac(6')-Ie-aph(2")-Ia*, and to compare their minimum inhibitory concentration (MIC) antibacterial efficacy with that of the flavonoid extract alone. With a low MIC of 18.75 µg/mL, AVCSNPs demonstrated stronger antibacterial activity than the flavonoid extract, which had a MIC of 50 µg/mL. The *mecA* gene was downregulated by AVCSNPs by –14.64 log2-fold, revealing a primary mechanism of action. The *mecA* gene, the primary resistance mechanism in methicillin-resistant *S. aureus*, may be circumvented by nanoparticles. The expression of the *aac(6')-Ie-aph(2")-Ia* gene decreased by –3.37 log2-fold. By disrupting key resistance genes, AVCSNPs, a biocompatible alternative to conventional antibiotics, may be able to treat MRSA infections.

6. Acknowledgements

The authors extend their appreciation to the Ministry of Higher Education and Scientific Research for their support. No funding was received.

7. Abbreviations

Abbreviation	Full Term
AMR	Antimicrobial Resistance
AVCSNPs	Aloe Vera Flavonoid-Loaded Chitosan Nanoparticles
CLSI	Clinical and Laboratory Standards Institute
CSNPs	Chitosan Nanoparticles
Ct	Cycle Threshold
DLS	Dynamic Light Scattering
DMSO	Dimethyl Sulfoxide
ddH_2O	Double-Distilled Water
FTIR	Fourier Transform Infrared Spectroscopy
HPLC	High-Performance Liquid Chromatography
MBC	Minimum Bactericidal Concentration
MDR	Multidrug-Resistant
MGEs	Mobile Genetic Elements
MHB	Mueller-Hinton Broth
MIC	Minimum Inhibitory Concentration
MRSA	Methicillin-Resistant *Staphylococcus aureus*
MSSA	Methicillin-Sensitive *Staphylococcus aureus*
PCR	Polymerase Chain Reaction
PDI	Polydispersity Index
qRT-PCR	Quantitative Real-Time Polymerase Chain Reaction
rRNA	Ribosomal RNA
TBE	Tris-Borate-EDTA Buffer
TPP	Sodium Tripolyphosphate
UV-Vis	Ultraviolet–Visible Spectroscopy
WHO	World Health Organization
XDR	Extensively Drug-Resistant
XRD	X-ray Diffraction

8. CRediT Statement

Saba Mejdhab Badr: Resources, Investigation, Data Curation, Writing – Original Draft, Visualization.
Rana A.H. Al-Lami: Conceptualization, Methodology, Validation, Supervision, Writing – Review & Editing.
Hanady S. Al-Shmgani: Conceptualization, Methodology, Validation, Supervision, Writing – Review & Editing

9. References

Akdaşçi, E., Duman, H., Eker, F., Bechelany, M., & Karav, S. (2025). Chitosan and its nanoparticles: A multifaceted approach to antibacterial applications. *Nanomaterials, 15*(2), Article 126. https://doi.org/10.3390/nano15020126

Ali, A. H. (2022). High-performance liquid chromatography (HPLC): A review. *Annals of Advances in Chemistry*, *6*(1), 10-20. https://doi.org/10.29328/journal.*aac.*1001026

Ali, M. R., & Khudhair, A. M. (2018). Detection of colony adhesion factors and genetic background of adhesion genes among multidrug-resistant uropathogenic *Escherichia coli* Isolated in Iraq. *Journal of Pure and Applied Microbiology*, *12*(4), 2017-2025. https://doi.org/10.22207/JPAM.12.4.38

Al-Khafaji, M. M. S., & Al-Hayawi, A. Y. (2024). Deciphering the impact of miR-92a-3p on controlling BCL11A gene expression and its implication in easing thalassemia symptoms. *Medical Journal of Babylon*, *21*(Suppl 2), S250-S257. https://doi.org/10.4103/MJBL.MJBL_1337_23

Al-Kubaisi, Z. A., Al-Shmgani, H. S., & Salman, M. J. (2020). Evaluation of in vivo and in vitro protective effects of quercetin on lipopolysaccharide-induced inflammation and cytotoxicology. *Research Journal of Pharmacy and Technology*, *13*(8), 3897-3902. http://doi.org/10.5958/0974-360X.2020.00690.3

AL-Lami, R. A., Al-Hayanni, H. S., & Shehab, Z. H. (2022). Molecular investigation of some beta-lactamase genes by PCR and DNA sequencing techniques in clinical *Escherichia coli*. *Iraqi Journal of Science*, *63*(10), 4205-4212. https://doi.org/10.24996/ijs.2022.63.10.7

Al-Musawi, M. M., Al-Bairuty, G. A., & Al-Shmgani, H. S. (2022). The comparative effect of copper oxide nanoparticles and copper sulfate on reproductive hormones and sperm parameters in mature male albino mice. *Annals of Biology*, *38*(2), 317-321. https://doi.org/10.1155/2022/4877637

Aldhahir, S., Al-Rayahi, I. A. M., & Muhsin, S. S. (2025). Comparison of myxovirus resistance gene 2 expression among adult and juvenile SLE Iraqi patients. *Journal of Current Science and Technology*, *15*(2), Article 97. https://doi.org/10.59796/jcst.V15N2.2025.97

Amini, S., Omidi, A. H., Afkhami, H., Sabati, H., Mohsenzadeh, A., Soleymani, A., ... & Mohammadi, M. R. (2024). Frequency of *aac(6´)-le-aph (2´´)* gene and resistance to Aminoglycoside antibiotics in *Staphylococcus aureus* isolates. *Cellular, Molecular and Biomedical Reports*, *4*(2), 120-128. https://doi.org/10.55705/cmbr.2023.411361.1166

Ausaj, A. A., Al-Shmgani, H. S., Abid, W. B., Gadallah, A. A., Mashlawi, A. M., Khormi, M. A., ... & Abada, E. (2024). Immobilization of bromelain on gold nanoparticles for comprehensive detection of their antioxidant, anti-angiogenic, and wound-healing potentials. *Inorganics*, *12*(12), Article 325. https://doi.org/10.3390/inorganics12120325

Bouslamti, M., El Barnossi, A., Kara, M., Alotaibi, B. S., Al Kamaly, O., Assouguem, A., ... & Benjelloun, A. S. (2022). Total polyphenols content, antioxidant and antimicrobial activities of leaves of *Solanum elaeagnifolium* Cav. from Morocco. *Molecules*, *27*(13), Article 4322. https://doi.org/10.3390/molecules27134322

Choi, S. M., Kim, S. H., Kim, H. J., Lee, D. G., Choi, J. H., Yoo, J. H., ... & Kang, M. W. (2003). Multiplex PCR for the detection of genes encoding aminoglycoside modifying enzymes and methicillin resistance among Staphylococcus species. *Journal of Korean Medical Science*, *18*(5), Article 631. https://doi.org/10.3346/jkms.2003.18.5.631

Cushnie, T. T., & Lamb, A. J. (2011). Recent advances in understanding the antibacterial properties of flavonoids. *International Journal of Antimicrobial Agents*, *38*(2), 99-107. https://doi.org/10.1016/j.ijantimicag.2011.02.014

Eckmann, C., & Dryden, M. (2010). Treatment of complicated skin and soft-tissue infections

caused by resistant bacteria: Value of linezolid, tigecycline, daptomycin and vancomycin. *European Journal of Medical Research*, *15*(12), Article 554. https://doi.org/10.1186/2047-783X-15-12-554

El-Naggar, N. E. A., Shiha, A. M., Mahrous, H., & Mohammed, A. A. (2022). Green synthesis of chitosan nanoparticles, optimization, characterization and antibacterial efficacy against multi drug resistant biofilm-forming *Acinetobacter baumannii. Scientific Reports*, *12*(1), Article 19869. https://doi.org/10.1038/s41598-022-24303-5

Ender, M., McCallum, N., & Berger-Bächi, B. (2008). Impact of *mecA* promoter mutations on *mecA* expression and β-lactam resistance levels. *International Journal of Medical Microbiology*, *298*(7-8), 607-617. https://doi.org/10.1016/j.ijmm.2008.01.015

Faiq, N. H., & Ahmed, M. E. (2024). Inhibitory effects of biosynthesized copper nanoparticles on biofilm formation of Proteus mirabilis. *Iraqi Journal of Science*, *65*(1), 65-78. https://doi.org/10.24996/ijs.2024.64.1.7

Fishovitz, J., Hermoso, J. A., Chang, M., & Mobashery, S. (2014). Penicillin-binding protein 2a of methicillin-resistant Staphylococcus aureus. *International Union of Biochemistry and Molecular Biology life*, *66*(8), 572-577. https://doi.org/10.1002/iub.1289

Gidamo, G. H. (2024). Stem cells of *Impatiens tinctoria* A. Rich tuber and antioxidant activity of their extracts. *Journal of Current Science and Technology*, *14*(3), Article 59. https://doi.org/10.59796/jcst.V14N3.2024.59

Hauschild, T., Sacha, P., Wieczorek, P., Zalewska, M., Kaczyńska, K., & Tryniszewska, E. (2008). Aminoglycosides resistance in clinical isolates of *Staphylococcus aureus* from a University Hospital in Bialystok, Poland. *Folia Histochemica et Cytobiologica*, *46*(2), 225-228. https://doi.org/10.2478/v10042-008-0034-3

Huanbutta, K., Sriamornsak, P., Suwanpitak, K., Klinchuen, N., Deebugkum, T., Teppitak, V., & Sangnim, T. (2023). Key fabrications of chitosan nanoparticles for effective drug delivery using flow chemistry reactors. *International Journal of Nanomedicine*, *18*, 7889–7900. https://doi.org/10.2147/IJN.S433756

Humphries, R., Bobenchik, A. M., Hindler, J. A., & Schuetz, A. N. (2021). Overview of changes to the Clinical and Laboratory Standards Institute performance standards for antimicrobial susceptibility testing, M100, 31st edition. *Journal of Clinical Microbiology*, *59*(10), Article e00213-21. https://doi.org/10.1128/jcm.00213-21

Hussain, A. I., Anwar, F., Nigam, P. S., Sarker, S. D., Moore, J. E., Rao, J. R., & Mazumdar, A. (2011). Antibacterial activity of some Lamiaceae essential oils using resazurin as an indicator of cell growth. *LWT-Food Science and Technology*, *44*(4), 1199-1206. https://doi.org/10.1016/j.lwt.2010.10.005

Jafar, F. N., & Sabah, F. S. (2024). Isolation of a flavonoid bioactive compound from *Gymnoascus dankaliensis* Secondary Metabolite. *Iraqi Journal of Science*, *65*(12), 6932-6945. https://doi.org/10.24996/ijs.2024.65.12.11

Jirakitticharoen, S., Wisuitiprot, W., Jitareerat, P., & Wongs-Aree, C. (2022). Phenolics, antioxidant and antibacterial activities of immature and mature *Blumea balsamifera* leaf extracts eluted with different solvents. *Journal of Tropical Medicine*, *2022*(1), Article 7794227. https://doi.org/10.1155/2022/7794227

Kadium, S. W., & Sahib, R. A. (2023). Antifungal activity of phenols compound separated from *quercus infectoria* and *citrullus colocynthis* against toxic fungi. *Archives of Razi Institute*, *78*(1), Article 297. https://doi.org/10.22092/ARI.2022.358960.2347

Karuncharoenpanich, T., Phetmanee, T., Pradubyat, N., Songsak, T., Jongrungruangchok, S., Madaka, F., Wunnakup, T., & Lakkana, N. (2025). In vitro assessment of antimicrobial activity and synergistic effects of ethanolic extracts from six medicinal plants. *Journal of Current Science and Technology, 15*(1), Article 85. https://doi.org/10.59796/jcst.V15N1.2025.85

Kiani, D. (2023). X-ray diffraction (XRD). *Springer Handbook of Advanced Catalyst Characterization*. Cham, Switzerland: Springer International Publishing. https://doi.org/10.1007/978-3-031-07125-6_25

Mehrotra, M., Wang, G., & Johnson, W. M. (2000). Multiplex PCR for detection of genes for *Staphylococcus aureus* enterotoxins, exfoliative toxins, toxic shock syndrome toxin 1, and methicillin resistance. *Journal of Clinical Microbiology*, *38*(3), 1032-1035. https://doi.org/10.1128/jcm.38.3.1032-1035.2000

Mendem, S. K., Alasthimannahalli Gangadhara, T., Shivannavar, C. T., & Gaddad, S. M. (2016). Antibiotic resistance patterns of *Staphylococcus aureus*: A multi-centre study from India. *Microbial Pathogenesis, 98*, 167–170. https://doi.org/10.1016/j.micpath.2016.07.010

Mishra, B. B. T. S., Patel, B. B., & Tiwari, S. (2010). Colloidal nanocarriers: A review on formulation technology, types and applications toward targeted drug delivery. *Nanomedicine: Nanotechnology, Biology and Medicine*, *6*(1), 9-24. https://doi.org/10.1016/j.nano.2009.04.008

Morovat, T., Bahram, F., Mohammad, E., Setareh, S., & Mohamad Mehdi, F. (2009). Distribution of different carbapenem resistant clones of Acinetobacter baumannii in Tehran hospitals. *The New Microbiologica*, *32*(3), 265-271.

O'Brien, J., Wilson, I., Orton, T., & Pognan, F. (2000). Investigation of the Alamar Blue (resazurin) fluorescent dye for the assessment of mammalian cell cytotoxicity. *European Journal of Biochemistry*, *267*(17), 5421–5426. https://doi.org/10.1046/j.1432-1327.2000.01606.x

Prisa, D. (2022). Aloe: Medicinal properties and botanical characteristics. *Journal of Current Science and Technology, 12*(3), 605–614. https://doi.org/10.14456/jcst.2022.46

Rahman, A., Kafi, M. A., Beak, G., Saha, S. K., Roy, K. J., Habib, A., ... & Choi, J. W. (2024). Green-synthesized chitosan nanoparticles for controlling multidrug-resistant *mecA*-and blaZ-positive *Staphylococcus aureus* and *aadA1*-positive *Escherichia coli*. *International Journal of Molecular Sciences*, *25*(9), Article 4746. https://doi.org/10.3390/ijms25094746

Urtgam, S., Thawathotsapakorn, S., & Wattanachaiyingcharoen, W. (2024). The partial nucleotide sequences of the mitochondrial genes, *COI* and *16S rRNA*, of fireflies in the genera *Pygoluciola*, *Trisinuata*, and *Medeopteryx* (Coleoptera: Lampyridae). *Journal of Current Science and Technology, 14*(2), Article 22. https://doi.org/10.59796/jcst.V14N2.2024.22

Vercelli, C., Amadori, M., Gambino, G., & Re, G. (2023). Does nitrofurantoin improve the portfolio of vets against resistant bacteria in companion animals?. *Antibiotics, 12*(5), Article 911. https://doi.org/10.3390/antibiotics12050911

Villarta, J. D. A., Paylago, F. J. C., Poldo, J. C. H., Santos, J. S. R., Escordial, T. A. M. M., & Montealegre, C. M. (2025). Green synthesis, characterization, and optimization of chitosan nanoparticles using *blumea balsamifera* extract. *Processes*, *13*(3), Article 804. https://doi.org/10.3390/pr13030804

World Health Organization. (2022). *Global antimicrobial resistance and use surveillance system (GLASS) report 2022*. Retrieved from https://apps.who.int/iris/handle/10665/364996

Zhang, D., Cui, K., Wang, T., Dong, H., Feng, W., Ma, C., & Dong, Y. (2018). Trends in and correlations between antibiotic consumption and resistance of *Staphylococcus aureus* at a tertiary hospital in China before and after introduction of an antimicrobial stewardship programme. *Epidemiology and Infection*, *147*, Article e48. https://doi.org/10.1017/S0950268818003059